Hierarchy of Lifshitz Transitions in the Surface Electronic Structure of Sr_2RuO_4 under Uniaxial Compression

Edgar Abarca Morales,[1,2] Gesa-R. Siemann,[2] Andela Zivanovic,[1,2] Philip A. E. Murgatroyd,[2] Igor Marković,[1,2,*] Brendan Edwards,[2] Chris A. Hooley,[2] Dmitry A. Sokolov,[1] Naoki Kikugawa,[3] Cephise Cacho,[4] Matthew D. Watson,[4] Timur K. Kim,[4] Clifford W. Hicks,[1,5] Andrew P. Mackenzie,[1,2] and Phil D. C. King[2,†]

[1]*Max Planck Institute for Chemical Physics of Solids, Nöthnitzer Strasse 40, 01187 Dresden, Germany*
[2]*SUPA, School of Physics and Astronomy, University of St Andrews, St Andrews KY16 9SS, United Kingdom*
[3]*National Institute for Materials Science, Tsukuba, Ibaraki 305-0003, Japan*
[4]*Diamond Light Source, Harwell Science and Innovation Campus, Didcot, OX11 ODE, United Kingdom*
[5]*School of Physics and Astronomy, University of Birmingham, Birmingham B15 2TT, United Kingdom*

(Received 23 July 2022; accepted 11 January 2023; published 27 February 2023)

We report the evolution of the electronic structure at the surface of the layered perovskite Sr_2RuO_4 under large in-plane uniaxial compression, leading to anisotropic B_{1g} strains of $\varepsilon_{xx} - \varepsilon_{yy} = -0.9 \pm 0.1\%$. From angle-resolved photoemission, we show how this drives a sequence of Lifshitz transitions, reshaping the low-energy electronic structure and the rich spectrum of van Hove singularities that the surface layer of Sr_2RuO_4 hosts. From comparison to tight-binding modeling, we find that the strain is accommodated predominantly by bond-length changes rather than modifications of octahedral tilt and rotation angles. Our study sheds new light on the nature of structural distortions at oxide surfaces, and how targeted control of these can be used to tune density of state singularities to the Fermi level, in turn paving the way to the possible realization of rich collective states at the Sr_2RuO_4 surface.

DOI: 10.1103/PhysRevLett.130.096401

A central building block of numerous correlated electron materials is the transition-metal-oxide octahedron. The distortions of coupled octahedra away from idealized cubic geometries underpin many of the striking physical properties which transition-metal oxides host. In perovskite nickelates, for example, tilts and rotations combined with breathinglike distortions of the NiO_6 octahedra support a rich phase diagram of metal-insulator and magnetic transitions [1,2]; in several titanates, off-centering of the Ti atom within the octahedral cage generates a ferroelectric state [3,4], while in some manganites, trilinear coupling of nonpolar tilt and rotation modes with polar displacements creates novel multiferroics [5]. In the ruthenate family, modest structural distortions drive the emergence of numerous correlated electron states [6–10]: unconventional superconductors [11], Mott insulators [12], polar metals [13], and quantum criticality [14] are all found in systems built around nominally the same RuO_6 structural unit. Disentangling the structure-property relations underpinning the formation of such disparate ground states is a major challenge in the field.

To this end, developing routes to observe modifications in electronic properties when structural distortions are tuned in a controlled manner is a key goal. Uniaxial pressure can provide such a control parameter [15–18], and can be applied in conjunction with spectroscopic probes [19–25]. In Sr_2RuO_4, for example, uniaxial compression has been shown to more than double its superconducting T_c and to stabilize T-linear resistivity [26,27]. Both effects have been attributed to a strain-driven Lifshitz transition in the electronic structure, where a saddle point van Hove singularity (vHS), and its associated peak in the density of states, is driven through the Fermi level [19,27].

Here we report the observation, from angle-resolved photoemission (ARPES), of the influence of uniaxial pressure on the surface electronic structure of Sr_2RuO_4. The Sr_2RuO_4 surface is known to distort via in-plane rotations of its RuO_6 octahedra, forming distinct electronic states with significantly more complex Fermi surfaces and low-energy electronic structures as compared with the bulk (Fig. 1) [28]. It thus serves as a benchmark system for probing the influence of small structural distortions on the electronic states. Our measurements and comparison with model calculations allow us to track how these are modified with strain. Through this, we show that bond-length distortions, not additional octahedral rotations, dominate the strain response in the surface layer, in turn mediating a rich sequence of surface Lifshitz transitions.

High-resolution ARPES measurements were performed using the I05 beamline at Diamond Light Source. Single-crystal samples were grown by the floating zone method [36]. Unlike in Ref. [19], where the samples were cleaved *ex situ* to remove signatures of surface states, here we cleave *in situ* at the measurement temperature of ≈7 K. This produces a clean surface with a well-ordered $\sqrt{2} \times \sqrt{2}$

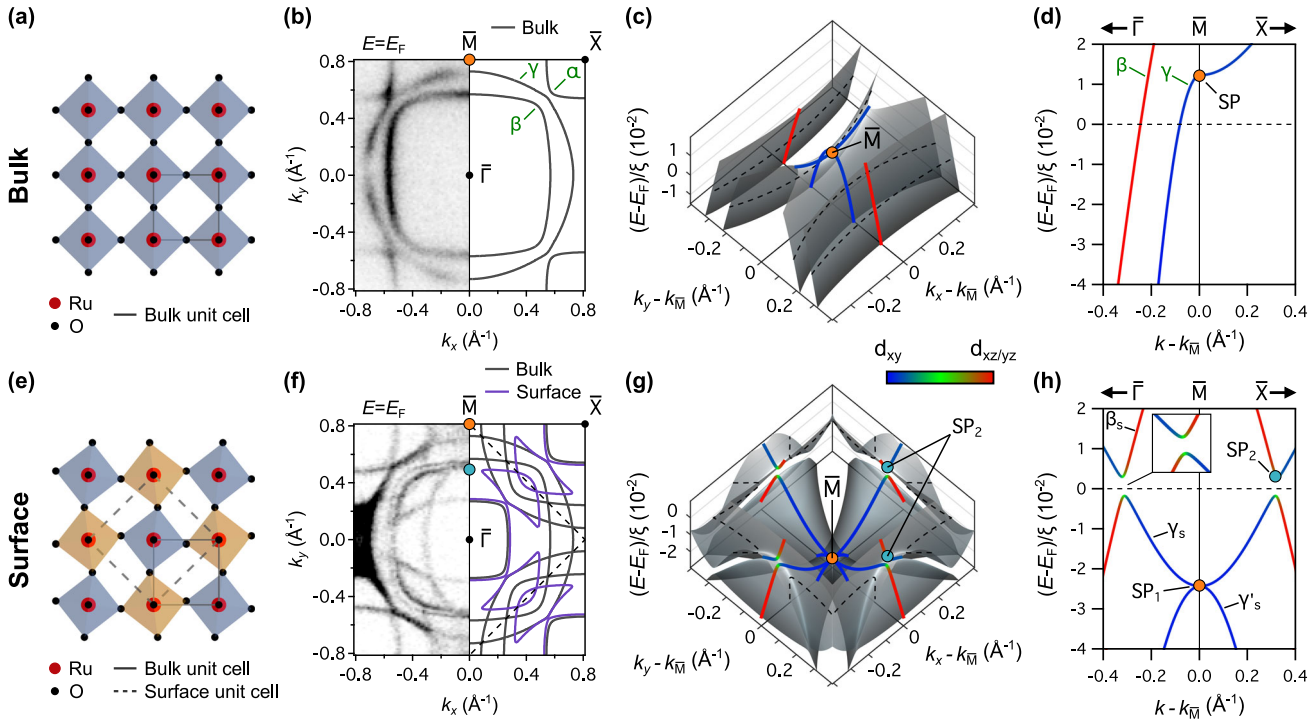

FIG. 1. (a) Top view of the RuO_2 layer of bulk Sr_2RuO_4. (b) Bulk Fermi surface measured using ARPES (left, reproduced from Ref. [19]) and calculated from our tight-binding model (right). (c) Calculated electronic structure in the vicinity of the $\overline{\mathrm{M}}$ point, showing the bulk vHS arising from the saddle point (SP) of the γ band. (d) Corresponding calculated dispersions along $\overline{\Gamma}$-$\overline{\mathrm{M}}$-$\overline{\mathrm{X}}$. (e) Bipartite RuO_2 layer of the surface of Sr_2RuO_4. (f) Surface Fermi surface measured with ARPES (left, $h\nu = 100$ eV, linear vertical polarisation) and calculated from a tight-binding model including the octahedral rotation (right). (g) and (h) Corresponding calculated electronic structure of the surface bands in the vicinity of the $\overline{\mathrm{M}}$ point. ξ is the bandwidth of the unstrained surface electronic structure (see Supplemental Material, Fig. S4 [29]).

reconstruction. Strain was applied through differential thermal contraction, using a compact, bimetallic platform described in Ref. [19] (see also Supplemental Material, Figs. S1(a)–S1(c) [29]). The induced anisotropic sample strain was characterized optically as shown in the Supplemental Material, Fig. S1(d) [29].

Sr_2RuO_4 is composed of single layers of corner-sharing RuO_6 octahedra [Fig. 1(a)], separated by SrO rocksalt layers. The conducting RuO_2 layers yield a quasi-two-dimensional three-band Fermi surface with states derived from the three partially occupied t_{2g} orbitals [Fig. 1(b)] [37]. In the surface layer, the RuO_6 octahedra are rotated about the c axis by ≈6–10° [38], in antiphase on neighboring sites [Fig. 1(e)] creating a 2 Ru-atom unit cell. The bulk states become backfolded about the new Brillouin zone boundary, while additional surface states are split off from the bulk manifold [Fig. 1(f)] [28,39]. Both the bulk and surface fermiology are well described by a simple tight-binding model, as shown in Figs. 1(b) and 1(f) and discussed in more detail in the Supplemental Material [29] (Figs. S2–S6).

We show in Figs. 2(a) and 2(b) the band dispersions of unstrained Sr_2RuO_4, measured along the high-symmetry $\overline{\Gamma}$-$\overline{\mathrm{M}}$ and $\overline{\mathrm{M}}$-$\overline{\mathrm{X}}$ directions. While distinct directions in the bulk, these are formally equivalent paths in the surface Brillouin zone (see insets). Nonetheless, the ARPES matrix elements vary significantly for measurements performed along these directions, and we will thus refer throughout to the conventional symmetry points of the surface Brillouin zone, with $\overline{\mathrm{M}}$ located at the $(\pi/a, 0)$ or $(0, \pi/a)$ points of the tetragonal Brillouin zone, and $\overline{\mathrm{X}}$ at $(\pi/a, \pi/a)$. Along $\overline{\Gamma}$-$\overline{\mathrm{M}}$, the hole band crossing E_F closest to the $\overline{\mathrm{M}}$ point in Fig. 2(a) is the bulk γ band [Fig. 1(b)], which is predominantly derived from d_{xy} orbitals. For such a two-dimensional d_{xy} band, a saddle point is expected at the $\overline{\mathrm{M}}$ point of the Brillouin zone [Figs. 1(c) and 1(d)]. While first-principle calculations suggest that its associated vHS should be located more than 60 meV above the Fermi level [40], electronic correlations renormalize this to only ≈14 meV above E_F [41–43]. Consistent with previous measurements [39], we find that a very weak replica of this band is also visible backfolded to the $\overline{\mathrm{M}}$-$\overline{\mathrm{X}}$ direction [Fig. 2(b)] due to the surface octahedral rotations.

Additional surface states are also evident. The saddle point of the surface γ band (SP_1) is pushed below the Fermi level [44] in the lower screening environment of the surface, with small additional downward shifts from band narrowing due to the octahedral rotation of the surface layer

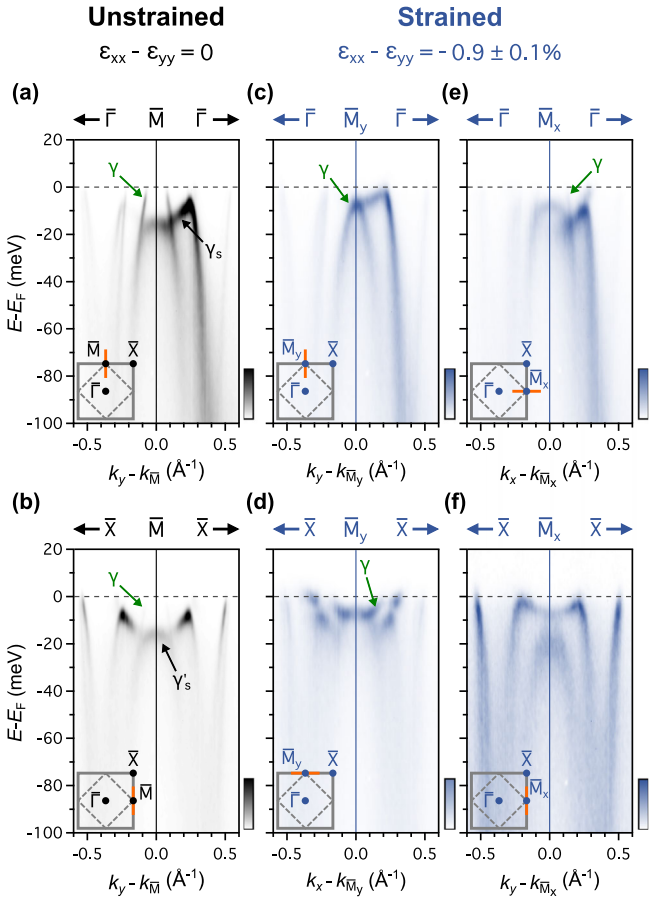

FIG. 2. Dispersions ($h\nu = 40$ eV, linear horizontal polarisation) close to the $\overline{\mathrm{M}}$ point of unstrained Sr_2RuO_4 measured along the (a) $\overline{\Gamma}$-$\overline{\mathrm{M}}$ and (b) $\overline{\mathrm{M}}$-$\overline{\mathrm{X}}$ directions. (c)–(f) Equivalent dispersions measured along the (c) $\overline{\Gamma}$-$\overline{\mathrm{M}}_y$, (d) $\overline{\mathrm{M}}_y$-$\overline{\mathrm{X}}$, (e) $\overline{\Gamma}$-$\overline{\mathrm{M}}_x$, and (f) $\overline{\mathrm{M}}_x$-$\overline{\mathrm{X}}$ direction for a strained sample ($\varepsilon_{xx} - \varepsilon_{yy} = -0.9 \pm 0.1\%$).

(see the Supplemental Material, Fig. S5 [29]). Moreover, the $\overline{\Gamma}$-$\overline{\mathrm{M}}$ and $\overline{\mathrm{M}}$-$\overline{\mathrm{X}}$ directions are folded onto each other by the doubling of the surface unit cell [Figs. 1(g) and 1(h)]. Experimentally, the signatures of this are visible in our measured dispersions in Figs. 2(a) and 2(b) as a degeneracy at $\overline{\mathrm{M}}$ of the electronlike (γ_s) and holelike (γ'_s) surface γ bands, located at a binding energy of 16 meV. The latter branch is most strongly visible along the $\overline{\mathrm{M}}$-$\overline{\mathrm{X}}$ direction [Fig. 2(b)], while the upward dispersing branch is clearly seen in the $\overline{\Gamma}$-$\overline{\mathrm{M}}$ measurements [Fig. 2(a)].

Interestingly, where γ_s crosses the surface β band (β_s), our tight-binding modeling [Fig. 1(h)] indicates that a small hybridization gap is opened by spin-orbit coupling [inset of Fig. 1(h); see also the Supplemental Material, Fig. S3 [29]]. The resulting band hybridization causes the formation of a new saddle point for the upper branch [SP_2 in Figs. 1(g) and 1(h)] while the lower branch develops a local band maximum. In our measurements of the surface electronic structure shown in Figs. 2(a) and 2(b), only the lower branch is visible in the occupied states, forming M-shaped bands along both $\overline{\mathrm{M}}$-$\overline{\Gamma}$ and $\overline{\mathrm{M}}$-$\overline{\mathrm{X}}$, which are gapped from the Fermi level by 7 ± 2 meV.

Significant changes in the electronic structure occur with uniaxial compression along the bulk Ru-O (x) direction (see also the Supplemental Material, Fig. S6 [29]). k_F of the bulk γ band is increased along the direction of applied compressive strain [we denote this as $\overline{\Gamma}$-$\overline{\mathrm{M}}_x$, Fig. 2(e)], while the γ band is pushed down below the Fermi level along the perpendicular $\overline{\Gamma}$-$\overline{\mathrm{M}}_y$ direction [Fig. 2(c)]. The band top along $\overline{\Gamma}$-$\overline{\mathrm{M}}_y$, and thus the position of its associated vHS, is now located 8 ± 2 meV below E_F, confirming our previous observation of a strain-induced bulk Lifshitz transition in Sr_2RuO_4 [19].

The evolution of the surface electronic structure is more complex. Along the $\overline{\Gamma}$-$\overline{\mathrm{M}}_y$ direction [Fig. 2(c), also visible along the symmetry-equivalent $\overline{\mathrm{X}}$-$\overline{\mathrm{M}}_x$ direction, Fig. 2(f)], the M-shaped band of the unstrained surface electronic structure [Figs. 2(a) and 2(b)] is pushed upward, reaching almost to the Fermi level. In contrast, along $\overline{\Gamma}$-$\overline{\mathrm{M}}_x$ [Fig. 2(e), and most clearly seen along the symmetry-equivalent $\overline{\mathrm{X}}$-$\overline{\mathrm{M}}_y$ direction, Fig. 2(d)], the same M-shaped band is pushed down, breaking the C_4 symmetry of the unstrained surface and leading to the initially unoccupied branch [Fig. 1(h)] moving below the Fermi level. A spin-orbit hybridization gap of ≈4 meV is now visible between the surface γ_s and β_s bands, centered ≈5 meV below the Fermi level.

To help visualize these strain-dependent changes, we show in Fig. 3 the surface band dispersions along the $\overline{\Gamma}$-$\overline{\mathrm{M}}_y$-$\overline{\mathrm{X}}$ direction. The dispersions in Fig. 3(b) are extracted from measurements performed using both linear horizontal [Figs. 2(c) and 2(d)] and vertical (Supplemental Material, Fig. S7 [29]) light polarization, where modified transition matrix elements better highlight the different band features (see also the Supplemental Material, Fig. S8 [29] for equivalent surface band dispersions extracted along the symmetry-equivalent $\overline{\mathrm{X}}$-$\overline{\mathrm{M}}_x$-$\overline{\Gamma}$ direction where the different experimental geometry again leads to distinct matrix elements). As well as confirming the surface Lifshitz transitions discussed above, these highlight an additional splitting of the originally fourfold degenerate vHS derived from the backfolded bands at $\overline{\mathrm{M}}$ into two distinct twofold degenerate saddle points, with the two branches split by ≈12 meV.

Our extracted dispersions thus point to a strong breaking of C_4 symmetry at the surface. This is naturally expected given the anisotropic strain; the details of how this reshapes the electronic structure, however, are less obvious. In the bulk, the effect of uniaxial stress is well understood in terms of a simple compression of the RuO_6 octahedra in the direction of the applied stress, with a corresponding bond-length expansion in the perpendicular direction due to the Poisson effect. At the surface, however, the RuO_6 octahedra are already rotated around the c axis in the absence of strain. The most natural starting assumption would

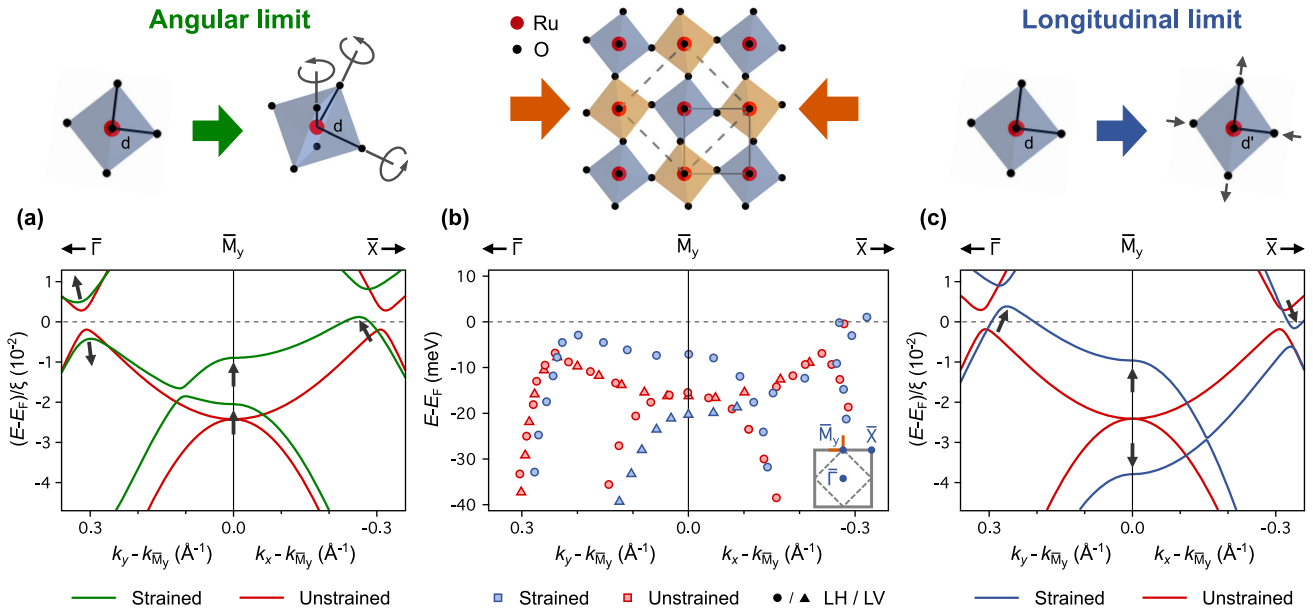

FIG. 3. Evolution of the surface electronic structure with uniaxial compression in the (a) angular and (c) longitudinal limits (see text). The dispersions extracted from our measured ARPES data using linear horizontal (LH) and vertical (LV) polarisation are shown in (b). The calculations employ a B_{1g} strain of $\varepsilon_{xx} - \varepsilon_{yy} = -2.4\%$, overestimating the experimental value as is also the case for bulk calculations [30,31] (see the Supplemental Material [29]).

therefore be that strain is accommodated by further rotations and tilts of these octahedra—we term this the *angular limit*. Assuming perfectly rigid octahedra, the rotations required to accommodate the strain are uniquely defined, and require a combination of in-plane rotation and out-of-plane octahedral tilting (see the Supplemental Material [29] and Figs. S9 and S10). From the resulting fully constrained changes in the geometrical configuration, we can directly calculate modifications of the interorbital hoppings within our tight-binding model, allowing us to predict the influence of the strain accommodation on the surface electronic structure without the introduction of any additional free parameters. We show the results of this in Fig. 3(a).

While the lowering of the symmetry of the surface electronic structure from C_4 to C_2 is, of course, reproduced by this model, we find that the strain-mediated changes in the electronic structure are otherwise in qualitative disagreement with our experimental measurements [Fig. 3(b)]. The top of the occupied M-shaped band is pushed upward toward the Fermi level along $\overline{\mathrm{M}}_y$-$\overline{\mathrm{X}}$, rather than the downward shift that is required to reproduce the surface Lifshitz transition observed experimentally. Meanwhile, along $\overline{\Gamma}$-$\overline{\mathrm{M}}_y$, the surface bands develop a strong hybridization gap, pushing the occupied states down well below the Fermi level, again in contrast to our experimental observations [Fig. 3(b)]. Finally, while the fourfold degenerate vHS at $\overline{\mathrm{M}}$ does become split under strain, both branches are split off above its position for the unstrained surface, distinct from the experimental situation where the new saddle points are split almost symmetrically about the unstrained case.

On the other hand, if we consider a *longitudinal limit*, where the surface octahedra are only able to distort via bond-length deformations, we predict an electronic structure which is in excellent agreement with our measured dispersions [Fig. 3(c)]. We thus conclude that application of uniaxial pressure to the bulk crystal leads, at least dominantly, to a change in Ru-O bond length of the surface octahedra.

We show in Fig. 4 how such strain-driven bond-length distortions additionally create a new Fermi pocket at the Brillouin zone center. We label this δ, in analogy with the corresponding Γ-centered Fermi pocket in $Sr_3Ru_2O_7$ [45]. Our tight-binding modeling [Figs. 4(d) and 4(e)] indicates that this δ band has predominantly d_{xy} and $d_{x^2-y^2}$ orbital character. The $d_{x^2-y^2}$ band is part of the e_g manifold, split off above the t_{2g} states by a large octahedral crystal field. For bulk Sr_2RuO_4, its hybridization with d_{xy} orbitals in the t_{2g} manifold is forbidden by symmetry. In the surface layer, however, the octahedral rotation permits their mixing (see the Supplemental Material, Fig. S5 [29]), leading to a local depression at the top of the backfolded surface γ band at $\overline{\Gamma}$. Consistent with prior work [44], our measurements of the unstrained sample indicate that the bottom of the resulting δ pocket is above the Fermi level. Our calculations, however, show that the $d_{xy}/d_{x^2-y^2}$ orbital mixing is enhanced under strain [Fig. 4(e)], lowering the energy of the bottom of the δ band [Figs. 4(d) and 4(e)], and in turn driving another Lifshitz transition leading to the creation of a new δ-pocket Fermi surface as observed experimentally [Figs. 4(a)–4(c)].

The fact that bond-length changes appear to dominate the structural response to an applied uniaxial stress here

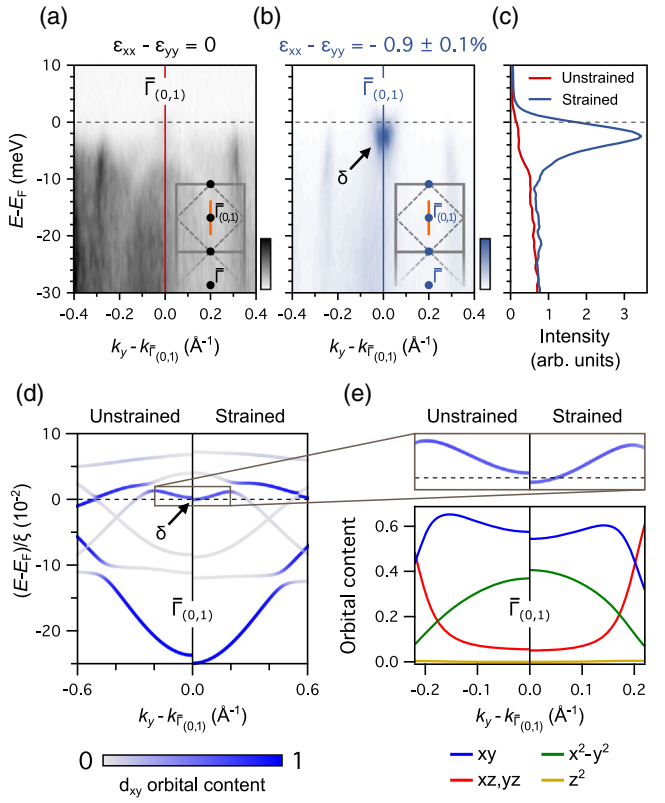

FIG. 4. Measured dispersions ($h\nu = 40$ eV, linear vertical polarisation) centered at the $\overline{\Gamma}$ point of the second Brillouin zone ($\overline{\Gamma}_{(0,1)}$) for (a) unstrained and (b) strained Sr_2RuO_4, and (c) $\overline{\Gamma}$-point energy distribution curves. (d) Tight-binding calculations showing the effect of strain within the longitudinal limit on the states near the Brillouin zone center, with projected d_{xy} orbital weight. (e) Magnified view of band dispersions in the vicinity of the new δ pocket (top), and corresponding d-orbital content (bottom).

may, at first sight, appear surprising, given the pre-existing surface reconstruction and the propensity of perovskite-type oxides to structural distortions involving octahedral rotations [1,46,47]. We note, however, that a Lifshitz transition itself can be expected to give a contribution to the electronic component of the compressibility [48], softening the lattice in line with the required bond-length changes that we find to dominate the structural distortions here. The hierarchy of Lifshitz transitions observed here under strain thus potentially provides an electronic incentive to favor bond-length distortion over rigid octahedral rotation, and motivates future study of the detailed strain-dependent distortions from surface-sensitive structural probes and first-principle calculations of surface structure under strain. Furthermore, we note that many of the other Ruddlesden-Popper ruthenates (and many perovskites in general) host octahedral rotations in their bulk crystal structure. Our findings thus motivate future studies for how strain—which can have a striking influence on their collective states [20,49–51]—modifies not just lattice constants, but also the local crystal structure in these systems. Beyond bulk systems, this is of interest for the study of epitaxial thin films, where biaxial strain can readily be coupled from a growth substrate, offering further opportunities for control [43].

Already at the surface, it may be possible to realize some of the rich phenomenology of the bulk systems using strain as a tuning parameter. In $Sr_3Ru_2O_7$, for example, field tuning of near-E_F vHSs, similar to those studied here, to the Fermi level is thought to drive the emergence of quantum criticality [14,52] and the stabilization of spin-density-wave phases [53]. Recent scanning tunneling microscopy measurements suggest that magnetic fields as high as 32 T would be required to achieve similar field-tuned Lifshitz transitions for the surface layer of Sr_2RuO_4 [54], while we have found here that the corresponding Lifshitz transition is naturally driven by modest applied uniaxial pressure. Moreover, we find that the M-shaped surface band which is pushed toward the Fermi level becomes flatter under the resulting strain [Fig. 2(c)], potentially mediating a cross-over to a so-called higher (fourth) order singularity, characterized by a power-law divergence in its associated density of states [55]. Such a "multicritical" singularity has been proposed as key to explaining the exotic collective states of the sister compound $Sr_3Ru_2O_7$. Our study, whereby a hierarchy of surface Lifshitz transitions is induced and tuned by an applied uniaxial stress, raises the tantalizing prospect that the surface of Sr_2RuO_4 could be driven to host its own quantum critical states, providing new possibilities for studying such phases with spectroscopic approaches.

The supporting data for this Letter are openly available from [56].

We thank J. Betouras, A. Chandrasekaran, D. Halliday, C. Marques, L. Rhodes, A. Rost, V. Sunko, and P. Wahl for useful discussions. We gratefully acknowledge support from the Engineering and Physical Sciences Research Council (Grants No. EP/T02108X/1 and No. EP/R031924/1), the European Research Council (through the QUESTDO Project No. 714193), and the Leverhulme Trust (Grant No. RL-2016-006). E. A. M., A. Z., and I. M. gratefully acknowledge studentship support from the International Max-Planck Research School for Chemistry and Physics of Quantum Materials. N. K. is supported by a KAKENHI Grants-in-Aids for Scientific Research (Grants No. 18K04715 and No. 21H01033), and Core-to-Core Program (No. JPJSCCA20170002) from the Japan Society for the Promotion of Science (JSPS) and by a JST-Mirai Program (Grant No. JPMJMI18A3). A. P. M. and C. W. H. acknowledge support from the Deutsche Forschungsgemeinschaft—TRR 288—422213477 (Project No. A10). Research in Dresden benefits from the environment provided by the DFG Cluster of

Excellence ct.qmat (EXC 2147, project ID 390858940). We thank Diamond Light Source for access to Beamline I05 (Proposals SI27471 and SI28412), which contributed to the results presented here.

*Present address: Quantum Matter Institute, University of British Columbia, Vancouver V6T 1Z4, British Columbia, Canada.
†pdk6@st-andrews.ac.uk

[1] J. B. Torrance, P. Lacorre, A. I. Nazzal, E. J. Ansaldo, and C. Niedermayer, Systematic study of insulator-metal transitions in perovskites $RNiO_3$ (R = Pr,Nd,Sm,Eu) due to closing of charge-transfer gap, Phys. Rev. B **45**, 8209 (1992).

[2] J. Varignon, M. N. Grisolia, J. Íñiguez, A. Barthélémy, and M. Bibes, Complete phase diagram of rare-earth nickelates from first-principles, npj Quantum Mater. **2**, 1 (2017).

[3] H. Takahasi, A note on the theory of barium titanate, J. Phys. Soc. Jpn. **16**, 1685 (1961).

[4] K. Tsuda, R. Sano, and M. Tanaka, Nanoscale local structures of rhombohedral symmetry in the orthorhombic and tetragonal phases of $BaTiO_3$ studied by convergent-beam electron diffraction, Phys. Rev. B **86**, 214106 (2012).

[5] N. A. Benedek and C. J. Fennie, Hybrid Improper Ferroelectricity: A Mechanism for Controllable Polarization-Magnetization Coupling, Phys. Rev. Lett. **106**, 107204 (2011).

[6] E. Dagotto, Complexity in strongly correlated electronic systems, Science **309**, 257 (2005).

[7] J. P. Carlo, T. Goko, I. M. Gat-Malureanu, P. L. Russo, A. T. Savici, A. A. Aczel, G. J. MacDougall, J. A. Rodriguez, T. J. Williams, G. M. Luke, C. R. Wiebe, Y. Yoshida, S. Nakatsuji, Y. Maeno, T. Taniguchi, and Y. J. Uemura, New magnetic phase diagram of $(Sr, Ca)_2RuO_4$, Nat. Mater. **11**, 323 (2012).

[8] J. E. Ortmann, J. Y. Liu, J. Hu, M. Zhu, J. Peng, M. Matsuda, X. Ke, and Z. Q. Mao, Competition Between Antiferromagnetism and Ferromagnetism in Sr_2RuO_4 Probed by Mn and Co Doping, Sci. Rep. **3**, 1 (2013).

[9] W. Lu, W. Dong Song, K. He, J. Chai, C. J. Sun, G. M. Chow, and J. S. Chen, The role of octahedral tilting in the structural phase transition and magnetic anisotropy in $SrRuO_3$ thin film, J. Appl. Phys. **113**, 063901 (2013).

[10] A. Herklotz, A. T. Wong, T. Meyer, M. D. Biegalski, H. N. Lee, and T. Z. Ward, Controlling octahedral rotations in a perovskite via strain doping, Sci. Rep. **6**, 1 (2016).

[11] A. P. Mackenzie, T. Scaffidi, C. W. Hicks, and Y. Maeno, Even odder after twenty-three years: The superconducting order parameter puzzle of Sr_2RuO_4, npj Quantum Mater. **2**, 1 (2017).

[12] S. Nakatsuji, S. I. Ikeda, and Y. Maeno, Ca_2RuO_4: New Mott Insulators of Layered Ruthenate, J. Phys. Soc. Jpn. **66**, 1868 (2013).

[13] S. Lei, M. Gu, D. Puggioni, G. Stone, J. Peng, J. Ge, Y. Wang, B. Wang, Y. Yuan, K. Wang, Z. Mao, J. M. Rondinelli, and V. Gopalan, Observation of quasi-two-dimensional polar domains and ferroelastic switching in a metal, $Ca_3Ru_2O_7$, Nano Lett. **18**, 3088 (2018).

[14] S. A. Grigera, R. S. Perry, A. J. Schofield, M. Chiao, S. R. Julian, G. G. Lonzarich, S. I. Ikeda, Y. Maeno, A. J. Millis, and A. P. Mackenzie, Magnetic field-tuned quantum criticality in the metallic ruthenate $Sr_3Ru_2O_7$, Science **294**, 329 (2001).

[15] S. I. Ikeda, S. Koiwai, Y. Yoshida, N. Shirakawa, S. Hara, M. Kosaka, and Y. Uwatoko, Magnetization of single crystalline strontium ruthenate under uniaxial-pressure, J. Magn. Magn. Mater. **272–276**, E293 (2004).

[16] S. I. Ikeda, N. Shirakawa, T. Yanagisawa, Y. Yoshida, S. Koikegami, S. Koike, M. Kosaka, and Y. Uwatoko, Uniaxial-pressure induced ferromagnetism of enhanced paramagnetic $Sr_3Ru_2O_7$, J. Phys. Soc. Jpn. **73**, 1322 (2013).

[17] C. W. Hicks, D. O. Brodsky, E. A. Yelland, A. S. Gibbs, J. A. Bruin, M. E. Barber, S. D. Edkins, K. Nishimura, S. Yonezawa, Y. Maeno, and A. P. Mackenzie, Strong increase of T_c of Sr_2RuO_4 under both tensile and compressive strain, Science **344**, 283 (2014).

[18] H. H. Kim, S. M. Souliou, M. E. Barber, E. Lefrançois, M. Minola, M. Tortora, R. Heid, N. Nandi, R. A. Borzi, G. Garbarino, A. Bosak, J. Porras, T. Loew, M. König, P. M. Moll, A. P. Mackenzie, B. Keimer, C. W. Hicks, and M. Le Tacon, Uniaxial pressure control of competing orders in a high-temperature superconductor, Science **362**, 1040 (2018).

[19] V. Sunko, E. Abarca Morales, I. Marković, M. E. Barber, D. Milosavljević, F. Mazzola, D. A. Sokolov, N. Kikugawa, C. Cacho, P. Dudin, H. Rosner, C. W. Hicks, P. D. C. King, and A. P. Mackenzie, Direct observation of a uniaxial stress-driven Lifshitz transition in Sr_2RuO_4, npj Quantum Mater. **4**, 1 (2019).

[20] S. Riccò, M. Kim, A. Tamai, S. McKeown Walker, F. Y. Bruno, I. Cucchi, E. Cappelli, C. Besnard, T. K. Kim, P. Dudin, M. Hoesch, M. J. Gutmann, A. Georges, R. S. Perry, and F. Baumberger, In situ strain tuning of the metal-insulator-transition of Ca_2RuO_4 in angle-resolved photoemission experiments, Nat. Commun. **9**, 1 (2018).

[21] D. Flötotto, Y. Bai, Y. H. Chan, P. Chen, X. Wang, P. Rossi, C. Z. Xu, C. Zhang, J. A. Hlevyack, J. D. Denlinger, H. Hong, M. Y. Chou, E. J. Mittemeijer, J. N. Eckstein, and T. C. Chiang, In situ strain tuning of the dirac surface states in Bi_2Se_3 films, Nano Lett. **18**, 5628 (2018).

[22] C. Lin *et al.*, Visualization of the strain-induced topological phase transition in a quasi-one-dimensional superconductor $TaSe_3$, Nat. Mater. **20**, 1093 (2021).

[23] P. D. C. King, Controlling topology with strain, Nat. Mater. **20**, 1046 (2021).

[24] D. V. Potapenko, Z. Li, J. W. Kysar, and R. M. Osgood, Nanoscale strain engineering on the surface of a bulk TiO_2 crystal, Nano Lett. **14**, 6185 (2014).

[25] C. M. Yim, C. Trainer, R. Aluru, S. Chi, W. N. Hardy, R. Liang, D. Bonn, and P. Wahl, Discovery of a strain-stabilised smectic electronic order in LiFeAs, Nat. Commun. **9**, 1 (2018).

[26] A. Steppke, L. Zhao, M. E. Barber, T. Scaffidi, F. Jerzembeck, H. Rosner, A. S. Gibbs, Y. Maeno, S. H. Simon, A. P. Mackenzie, and C. W. Hicks, Strong peak in T_c of Sr_2RuO_4 under uniaxial pressure, Science **355**, 148 (2017).

[27] M. E. Barber, A. S. Gibbs, Y. Maeno, A. P. Mackenzie, and C. W. Hicks, Resistivity in the Vicinity of a van Hove Singularity: Sr_2RuO_4 under Uniaxial Pressure, Phys. Rev. Lett. **120**, 076602 (2018).

[28] A. Damascelli, D. H. Lu, K. M. Shen, N. P. Armitage, F. Ronning, D. L. Feng, C. Kim, Z. X. Shen, T. Kimura, Y. Tokura, Z. Q. Mao, and Y. Maeno, Fermi Surface, Surface States, and Surface Reconstruction in Sr_2RuO_4, Phys. Rev. Lett. **85**, 5194 (2000).

[29] See Supplemental Material at http://link.aps.org/supplemental/10.1103/PhysRevLett.130.096401 for sample strain characterisation, additional details of, and results from, our tight-binding and structural modelling, and additional data and analysis, and which includes Refs. [19,30–35].

[30] M. E. Barber, F. Lechermann, S. V. Streltsov, S. L. Skornyakov, S. Ghosh, B. J. Ramshaw, N. Kikugawa, D. A. Sokolov, A. P. Mackenzie, C. W. Hicks, and I. I. Mazin, Role of correlations in determining the Van Hove strain in Sr_2RuO_4, Phys. Rev. B **100**, 245139 (2019).

[31] S. Acharya, D. Pashov, C. Weber, H. Park, L. Sponza, and M. van Schilfgaarde, Evening out the spin and charge parity to increase T_c in Sr_2RuO_4, Commun. Phys. **2**, 163 (2019).

[32] J. J. Sakurai, *Modern Quantum Mechanics*, revised ed., edited by S. F. Tuan (Addison-Wesley, Reading, Massachusetts, 1994).

[33] H. Qian, Z. Yu, C. Lyu, F. Chen, Y. Luo, Y. Liu, M. Mao, and Y. Lyu, Easy-to-use model to reveal the nature of octahedral rotation transformations in perovskites, Ceram. Int. **46**, 4477 (2020).

[34] E. T. Filipov, K. Liu, T. Tachi, M. Schenk, and G. H. Paulino, Bar and hinge models for scalable analysis of origami, Int. J. Solids Struct. **124**, 26 (2017).

[35] P. Berner, Technical concepts: Orientation, rotation, velocity, and acceleration, and the SRM, Technical Report (TENA (Test & Training Enabling Architecture) project by SEDRIS 21, 2008).

[36] J. S. Bobowski, N. Kikugawa, T. Miyoshi, H. Suwa, H. S. Xu, S. Yonezawa, D. A. Sokolov, A. P. Mackenzie, and Y. Maeno, Improved single-crystal growth of Sr_2RuO_4, Condens. Matter **4**, 6 (2019).

[37] A. P. Mackenzie, S. R. Julian, A. J. Diver, G. J. McMullan, M. P. Ray, G. G. Lonzarich, Y. Maeno, S. Nishizaki, and T. Fujita, Quantum Oscillations in the Layered Perovskite Superconductor Sr_2RuO_4, Phys. Rev. Lett. **76**, 3786 (1996).

[38] R. Matzdorf, Ismail, T. Kimura, Y. Tokura, and E. W. Plummer, Surface structural analysis of the layered perovskite Sr_2RuO_4 by LEED I(V), Phys. Rev. B **65**, 085404 (2002).

[39] C. N. Veenstra, Z. H. Zhu, B. Ludbrook, M. Capsoni, G. Levy, A. Nicolaou, J. A. Rosen, R. Comin, S. Kittaka, Y. Maeno, I. S. Elfimov, and A. Damascelli, Determining the Surface-to-Bulk Progression in the Normal-State Electronic Structure of Sr_2RuO_4 by Angle-Resolved Photoemission and Density Functional Theory, Phys. Rev. Lett. **110**, 097004 (2013).

[40] C. Autieri, M. Cuoco, and C. Noce, Structural and electronic properties of $Sr_2RuO_4/Sr_3Ru_2O_7$ heterostructures, Phys. Rev. B **89**, 075102 (2014).

[41] K. M. Shen, N. Kikugawa, C. Bergemann, L. Balicas, F. Baumberger, W. Meevasana, N. J. C. Ingle, Y. Maeno, Z. X. Shen, and A. P. Mackenzie, Evolution of the Fermi Surface and Quasiparticle Renormalization through a van Hove Singularity in $Sr_{2-y}La_yRuO_4$, Phys. Rev. Lett. **99**, 187001 (2007).

[42] A. Tamai *et al.*, High-Resolution Photoemission on Sr_2RuO_4 Reveals Correlation-Enhanced Effective Spin-Orbit Coupling and Dominantly Local Self-Energies, Phys. Rev. X **9**, 021048 (2019).

[43] B. Burganov, C. Adamo, A. Mulder, M. Uchida, P. D. C. King, J. W. Harter, D. E. Shai, A. S. Gibbs, A. P. Mackenzie, R. Uecker, M. Bruetzam, M. R. Beasley, C. J. Fennie, D. G. Schlom, and K. M. Shen, Strain Control of Fermiology and Many-Body Interactions in Two-Dimensional Ruthenates, Phys. Rev. Lett. **116**, 197003 (2016).

[44] K. M. Shen, A. Damascelli, D. H. Lu, N. P. Armitage, F. Ronning, D. L. Feng, C. Kim, Z. X. Shen, D. J. Singh, I. I. Mazin, S. Nakatsuji, Z. Q. Mao, Y. Maeno, T. Kimura, and Y. Tokura, Surface electronic structure of Sr_2RuO_4, Phys. Rev. B **64**, 180502(R) (2001).

[45] A. Tamai, M. P. Allan, J. F. Mercure, W. Meevasana, R. Dunkel, D. H. Lu, R. S. Perry, A. P. Mackenzie, D. J. Singh, Z. X. Shen, and F. Baumberger, Fermi Surface and van Hove Singularities in the Itinerant Metamagnet $Sr_3Ru_2O_7$, Phys. Rev. Lett. **101**, 026407 (2008).

[46] G. Koster, L. Klein, W. Siemons, G. Rijnders, J. S. Dodge, C. B. Eom, D. H. A. Blank, and M. R. Beasley, Structure, physical properties, and applications of $SrRuO_3$ thin films, Rev. Mod. Phys. **84**, 253 (2012).

[47] I. Marković, M. D. Watson, O. J. Clark, F. Mazzola, E. A. Morales, C. A. Hooley, H. Rosner, C. M. Polley, T. Balasubramanian, S. Mukherjee, N. Kikugawa, D. A. Sokolov, A. P. Mackenzie, and P. D. C. King, Electronically driven spin-reorientation transition of the correlated polar metal $Ca_3Ru_2O_7$, Proc. Natl. Acad. Sci. U.S.A. **117**, 15524 (2020).

[48] I. Lifshitz, Anomalies of electron characteristics of a metal in the high pressure region, Sov. Phys. JETP **11**, 1130 (1960), http://jetp.ras.ru/cgi-bin/dn/e_011_05_1130.pdf.

[49] D. O. Brodsky, M. E. Barber, J. A. N. Bruin, R. A. Borzi, S. A. Grigera, R. S. Perry, A. P. Mackenzie, and C. W. Hicks, Strain and vector magnetic field tuning of the anomalous phase in $Sr_3Ru_2O_7$, Sci. Adv. **3**, e1501804 (2017).

[50] A. S. McLeod, A. Wieteska, G. Chiriaco, B. Foutty, Y. Wang, Y. Yuan, F. Xue, V. Gopalan, L. Q. Chen, Z. Q. Mao, A. J. Millis, A. N. Pasupathy, and D. N. Basov, Nano-imaging of strain-tuned stripe textures in a Mott crystal, npj Quantum Mater. **6**, 46 (2021).

[51] C. D. Dashwood, A. Walker, M. P. Kwasigroch, L. S. I. Veiga, Q. Faure, J. G. Vale, D. G. Porter, P. Manuel, D. D. Khalyavin, F. Orlandi, C. V. Colin, O. Fabelo, F. Krüger, R. S. Perry, R. D. Johnson, A. G. Green, and D. F. McMorrow, Strain control of a bandwidth-driven spin reorientation in $Ca_3Ru_2O_7$, arXiv:2210.12555.

[52] R. A. Borzi, S. A. Grigera, J. Farrell, R. S. Perry, S. J. Lister, S. L. Lee, D. A. Tennant, Y. Maeno, and A. P. Mackenzie, Formation of a nematic fluid at high fields in $Sr_3Ru_2O_7$, Science **315**, 214 (2007).

[53] C. Lester, S. Ramos, R. S. Perry, T. P. Croft, R. I. Bewley, T. Guidi, P. Manuel, D. D. Khalyavin, E. M. Forgan, and S. M. Hayden, Field-tunable spin-density-wave phases in $Sr_3Ru_2O_7$, Nat. Mater. **14**, 373 (2015).

[54] C. A. Marques, L. C. Rhodes, R. Fittipaldi, V. Granata, C. Ming Yim, R. Buzio, A. Gerbi, A. Vecchione, A. W. Rost, P. Wahl, C. A. Marques, L. C. Rhodes, C. M. Yim, A. W. Rost, P. Wahl, R. Fittipaldi, A. Vecchione, and V. Granata, Magnetic-field tunable intertwined checkerboard charge order and nematicity in the surface layer of Sr_2RuO_4, Adv. Mater. **33**, 2100593 (2021).

[55] D. V. Efremov, A. Shtyk, A. W. Rost, C. Chamon, A. P. Mackenzie, and J. J. Betouras, Multicritical Fermi Surface Topological Transitions, Phys. Rev. Lett. **123**, 207202 (2019).

[56] E. Abarca Morales, G. Siemann, A. Zivanovic, P. Murgatroyd, I. Markovic, B. Edwards, C. Hooley, D. Sokolov, N. Kikugawa, C. Cacho *et al.*, Hierarchy of Lifshitz transitions in the surface electronic structure of Sr2RuO4 under uniaxial compression (dataset), University of St Andrews Research Portal (2023), 10.17630/be3be544-f107-4863-93a3-eff656095c15.